ACSNANO

www.acsnano.org

ARTICLE

Preparation and Self-Assembly of Dendronized Janus Fe_3O_4–Pt and Fe_3O_4–Au Heterodimers

Davit Jishkariani,[†,‡,⊥] Yaoting Wu,[†,⊥] Da Wang,[∥,⊥] Yang Liu,[∥,#] Alfons van Blaaderen,[∥] and Christopher B. Murray*[,†,§]

[†]Department of Chemistry and [§]Department of Materials Science and Engineering, University of Pennsylvania, Philadelphia, Pennsylvania 19104, United States

[‡]Complex Assemblies of Soft Matter Laboratory (COMPASS), UMI 3254, CNRS-Solvay-University of Pennsylvania, CRTB, 350 George Patterson Boulevard, Bristol, Pennsylvania 19007, United States

[∥]Soft Condensed Matter, Debye Institute for Nanomaterials Science, Utrecht University, Princetonplein 5, 3584 CC Utrecht, The Netherlands

[#]Department of Earth Sciences, Utrecht University, Budapestlaan 4, 3584 CD Utrecht, The Netherlands

S *Supporting Information*

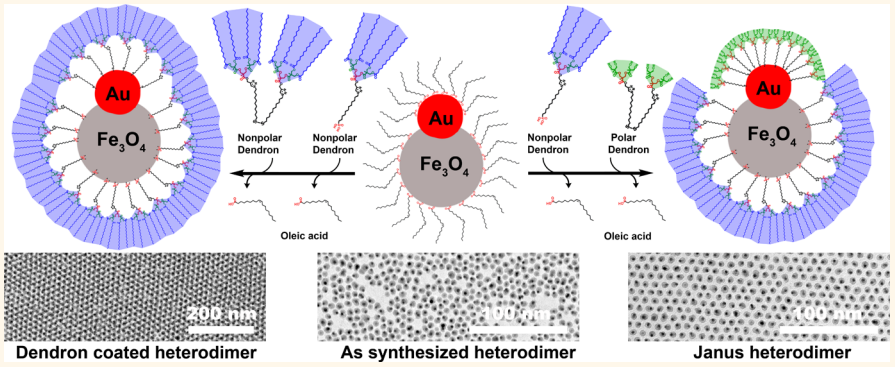

ABSTRACT: **Janus nanoparticles (NPs) often referred to as nanosized analogs of molecular surfactants are amphiphilic structures with potential applications in materials science, biomedicine, and catalysis, and their synthesis and self-assembly into complex architectures remain challenging. Here, we demonstrate the preparation of Janus heterodimers *via* asymmetric functionalization of Fe_3O_4–Pt and Fe_3O_4–Au heterodimeric NPs. The hydrophobic and hydrophilic dendritic ligands that carry phosphonic acid and disulfide surface binding groups selectively coat the iron oxide and platinum (or gold) parts of the heterodimer, respectively. Such an approach allows simple and efficient preparation of amphiphilic structures. Moreover, liquid–air interface self-assembly studies of each ligand exchange step revealed a drastic improvement in film crystallinity, suggesting the dendronization induced improvement of the whole particle polydispersity of the heterodimers.**

KEYWORDS: *Janus nanoparticles, heterodimers, dendritic ligands, ligand exchange, self-assembly*

Inorganic NPs are the main building blocks of nanotechnology and are under extensive research, as they provide distinctive physical properties which originate from their specific size, shape, composition, and surface chemistry that differ from those of bulk materials.[1−3] NPs find applications in broad areas such as electronic devices,[4,5] bioimaging,[6,7] data storage,[8,9] optical and chemical sensors,[10] and catalysis.[11,12] The successful implementation of NPs into devices requires two key aspects to be addressed: (i) well-controlled synthesis of nanosized building blocks and (ii) their self-assembly into functional architectures. Since the discovery of NPs, a great deal of research has been focused on methods that allow the preparation of NPs with different size, shape, and composition, which now leads to a fairly large collection of precise and reproducible synthetic and shape controlling methods.[13−16] On the other hand, the surface treatment is extremely important, as it is responsible for changes in their optical,[17] magnetic,[18] electronic,[19] and colloidal properties[20,21] as well as is key toward NP assemblies into different architectures.[22,23] To this end, the major surface treatment methods include formation or removal of organic monolayers formed by molecules such as commercially available surfac-

Received: April 10, 2017
Accepted: August 3, 2017
Published: August 3, 2017

DOI: 10.1021/acsnano.7b02485
ACS Nano 2017, 11, 7958–7966

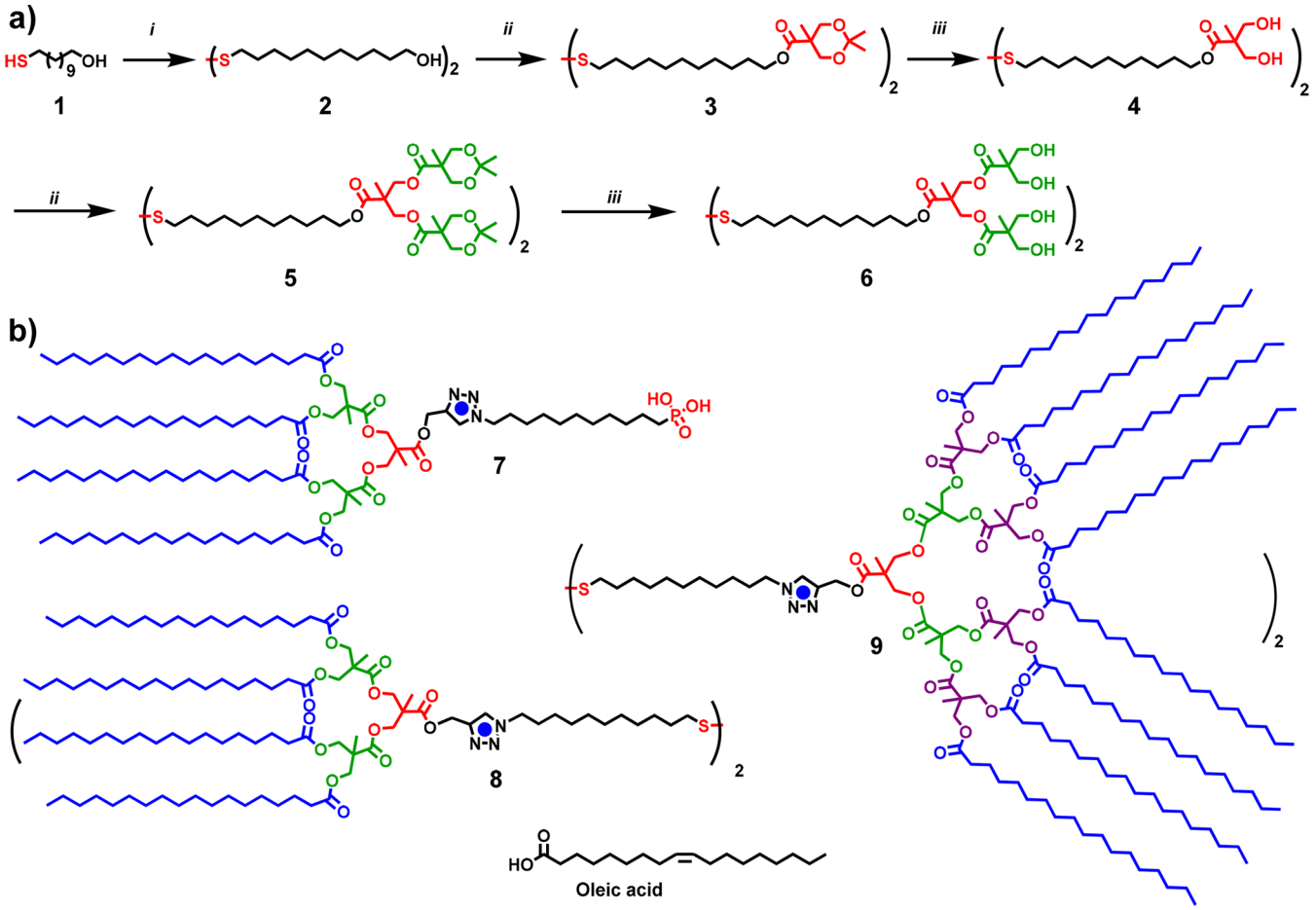

Figure 1. (a) The synthesis of hydrophilic dithiol dendron library and (b) the structures of hydrophobic phosphonic acid and dithiol dendrons. Reagents and conditions: (*i*) I_2, CH_2Cl_2, rt, 12 h; (*ii*) 2,2,5-trimethyl-1,3-dioxane-5-carboxylic anhydride, CH_2Cl_2, pyridine, DMAP, rt, 12 h; and (*iii*) Dowex (H^+), MeOH, 40 °C, 4 h.

tants,[24] DNA,[25] polymers,[26] and dendrimers.[17,20,27,28] Most of such surface modification methods allow a homogeneous treatment over an entire surface.

A particularly important recent development is control over directional interactions such as, for instance, becomes possible by the formation of amphiphilic systems where two types of ligands (hydrophobic and hydrophilic) are attached on different sides of particles to create a Janus particle commonly called after the two-faced Roman mythology god Janus.[29,30] The self-assembly of Janus particles can produce a series of more complex and delicate structures than isotropic building blocks and gives a deep understanding about anisotropic interactions and self-assembly mechanisms.[31] Literature methods for the preparation of Janus particles usually involve partial masking of a particle surface while functionalizing the exposed part of the surface. Functionalization methods include vapor deposition,[32] electrostatic deposition,[33] layer-by-layer self-assembly,[34] mechanical pressing,[35] and seeded emulsion polymerization.[36] Most of these methods are applied to micron- or submicron-sized particles. Reports on the preparation of nanometer-sized Janus particles are much rarer,[37−39] because the asymmetric modification visualization, characterization, and unambiguous verification of their Janus nature is a lot more challenging at the nanoscale.[38]

Herein, we present an efficient strategy for the preparation of solution processable Janus NPs through orthogonal functionalization of each inorganic component of nanosized Fe_3O_4−Pt and Fe_3O_4−Au heterodimeric particles with specifically designed dendritic ligands.

Heterodimers are two closely adjacent NPs that differ in size, shape, and/or in composition.[40−46] The surface modification of heterodimers was carried out as a two-step protocol where each inorganic component was functionalized through a solution-phase ligand exchange process.[47−50] Ligands with desired solubility properties and matching surface binding groups were accessed through organic synthesis, and the evidence of selective surface binding is obtained by energy dispersive X-ray spectroscopy (EDX) chemical mapping. Self-assembly characteristics of the NPs after each surface modification steps were studied by producing superlattice films on a liquid−air interface. Ligand exchange with orthogonally binding bulky monodisperse dendritic ligands revealed an increase in interparticle distances and a drastic improvement in film crystallinity compared to films made from untreated or partially treated particles, demonstrating the dendronization as an efficient tool to counterbalance the shape and size inhomogeneity and enhance their whole particle polydispersity.

RESULTS/DISCUSSION

To achieve an efficient yet orthogonal functionalization of Fe_3O_4−Pt and Fe_3O_4−Au heterodimeric NPs, we relied on different surface adhesion properties of phosphonic acid and sulfide-based head groups. It is well established that phosphonic

DOI: 10.1021/acsnano.7b02485
ACS Nano 2017, 11, 7958−7966

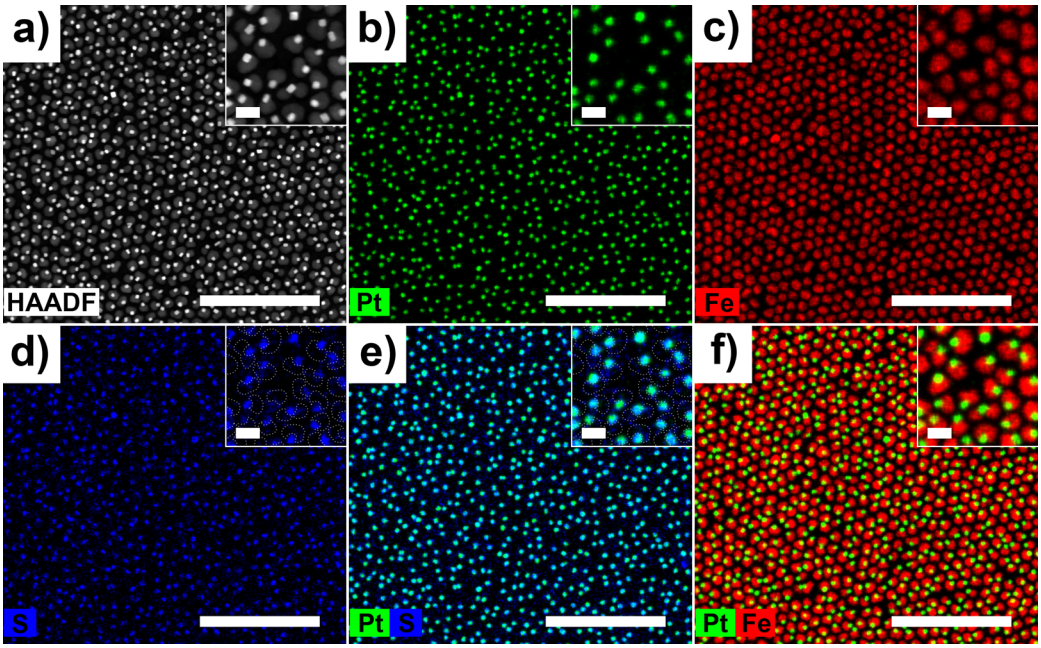

Figure 2. EDX chemical mapping of a Janus heterodimer superlattice (a) HAADF-STEM image of the area studied, (b) distribution of platinum, (c) distribution of iron, (d) distribution of sulfur, (e) superimposition of sulfur and platinum distribution, and (f) superimposition of iron and platinum distribution. For clarity, enlarged 100 nm × 100 nm areas are provided as insets in every image. Dashed lines in insets of (d) and (e) represent the Fe_3O_4 part and is provided for eye guide only. Scale bars in (a–f) are 200 nm. Scale bars in insets are 20 nm.

acids bind strongly to iron oxide and ferrite NP surfaces,[51,52] while sulfur-based head groups have higher affinity toward metallic NPs, such as Au, Ag, and Pt.[49,53,54] Therefore, it was clear that the successful orthogonal functionalization would require us to gain access to ligands with phosphonic acid and disulfide surface binding groups. A dendritic architecture was chosen as it provides a well-controlled synthetic platform where the bulkiness of the ligands and the nature and polyvalency of the end groups can be tuned independently from each other.[17,55−59]Disulfide dendrons with polar end-groups were envisioned to be based on 2,2-bis(hydroxymethyl)propionic acid (bis-MPA)-type dendron with free hydroxyl groups on the periphery, allowing the tuning of overall polarity by changing the number of hydroxyl groups as a function of dendrimer generation.[59−61] The designed route involves divergent synthesis through anhydride coupling starting from a building block 11-mercaptoundecan-1-ol **1**. This gives us access to a series of dendrons with a controlled number of hydroxyl end-groups (1, 2, and 4 per each sulfur atom) and therefore allows the tuning of polarity.

The thiol group of 11-mercaptoundecan-1-ol **1** was first protected by converting it into a disulfide *via* iodine-induced oxidation. Generation growth was ensured using a two-step procedure where the first step introduces the protected bis-MPA unit through 2,2,5-trimethyl-1,3-dioxane-5-carboxylic anhydride, and the second step removes the acetonide protecting groups using Dowex (H^+) acidic resin, thus affording compounds **3** and **4**.[17,60,61] Repeating this two-step sequence allowed formation of higher generations as shown on Figure 1a.

Disulfide ligands **2**, **4**, and **6** therefore represent zero-, first-, and second-generation dendrons (G0−2), where the number represents terminal hydroxyl end-groups, and therefore the polarity increases as a function of generation. These dendrons carry disulfide anchoring units which are used for functionalization of the Pt part of the heterodimers. As for the nonpolar counterpart, we considered a second-generation, stearate terminated, phosphonic acid bearing dendron **7** (Figure 1b).[62]

Janus particles were prepared through sequential ligand exchange of the Fe_3O_4−Pt (or Fe_3O_4−Au) heterodimers. The first ligand exchange step was carried out in the presence of an excess of the nonpolar dendron **7** at 35 °C in chloroform for 12 h to coat the Fe_3O_4 part. After which the particles were purified by precipitating with MeOH, collected by centrifugation, and redispersed in chloroform. The purification step was repeated three times to ensure the complete removal of any excess of dendron **7** and exchanged unbound original ligand, oleic acid. The second ligand exchange step was carried out under analogous conditions using polar disulfide dendrons **2**, **4**, or **6** (to form Janus particles) or using nonpolar dendrons **8** or **9** (to form nonpolar dendron-coated heterodimers). This step functionalizes the metal (Pt or Au) part of the heterodimer. The final hybrids can be purified by precipitating with excess MeOH and redispersing in chloroform. This process is also suitable for Janus particles as the Fe_3O_4 part of the dimeric NP is larger in size and the resulting Janus NP benefits from a large nonpolar part and can be dispersed in nonpolar solvents, which is key to carry out the self-assembly experiments.

To probe the effect of each ligand, their self-assembly behavior was studied after each ligand exchange step. The effect of the first ligand exchange step (using phosphonic acid **7** on Fe_3O_4−Pt heterodimers) was clearly seen from the significant increase in surface to the closest surface interparticle spacing (from 1.0 to 2.4 nm, as measured between two Fe_3O_4 bodies from TEM images). However, the direct proof of an asymmetric functionalization was obtained with EDX chemical mapping which was performed on the superlattice film made from particles bearing ligands **7** and **6** after the second ligand exchange step. Figure 2a shows the high-angle annular dark-field scanning transmission electron microscopy (HAADF-STEM) image of the area examined. Platinum and iron

DOI: 10.1021/acsnano.7b02485
ACS Nano 2017, 11, 7958−7966

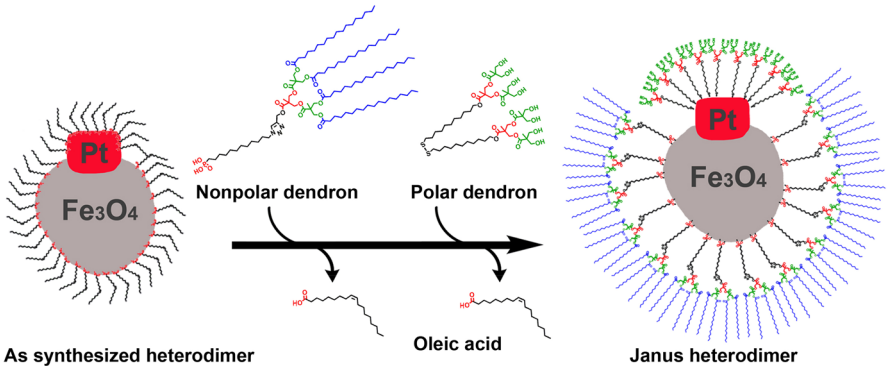

Figure 3. Schematic representation of the two-step ligand exchange process using dendritic ligands 7 and 6.

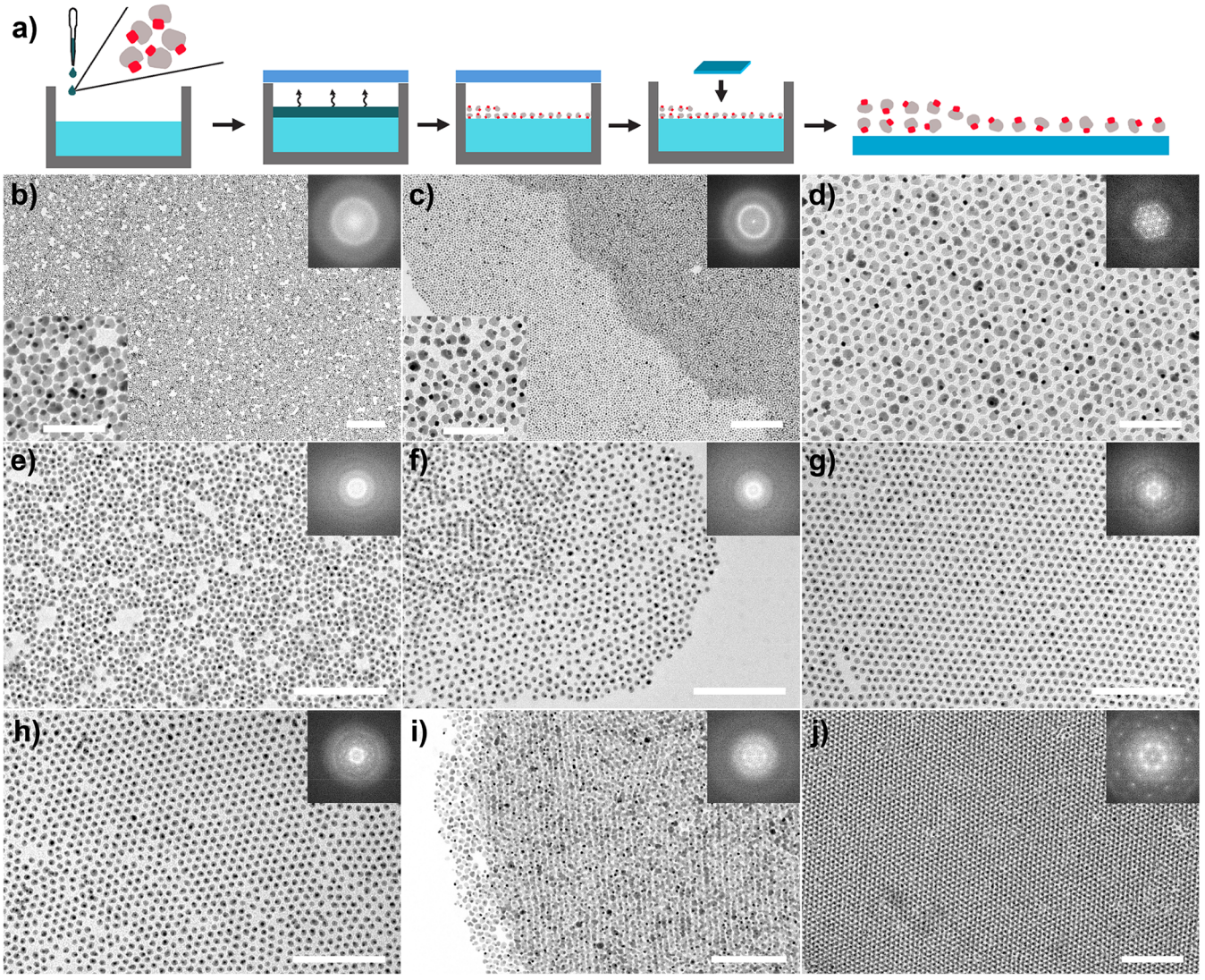

Figure 4. (a) Schematic representation of liquid–air assembly and sample preparation by "stamping" process. TEM images of (b) as-synthesized Fe_3O_4–Pt heterodimers (inset shows higher magnification area of the same sample), (c) Fe_3O_4–Pt heterodimers after functionalization of the Fe_3O_4 part with dendron 7 (inset shows higher magnification area of the same sample), (d) Fe_3O_4–Pt Janus heterodimers (prepared after functionalizing the Fe_3O_4 part with dendron 7 and the Pt part with dendron 6), (e) as-synthesized Fe_3O_4–Au heterodimers, (f) Fe_3O_4–Au heterodimers after functionalization of the Fe_3O_4 part with dendron 7, (g) Fe_3O_4–Au Janus heterodimers (after functionalizing the Fe_3O_4 part with dendron 7 and the Au part with dendron 6), (h) Fe_3O_4–Au heterodimers after functionalization of the Fe_3O_4 part with dendron 7 and the Au part with dendron 9, (i) a bilayer of Fe_3O_4–Pt Janus heterodimers (prepared after functionalizing the Fe_3O_4 part with dendron 7 and the Pt part with dendron 6), and (j) Fe_3O_4–Au heterodimers after functionalization of the Fe_3O_4 part with dendron 7 and the Au part with dendron 8. Scale bars in (b) and (c) 400 nm, in (d–h) 100 nm, and in (i) and (j) 200 nm. Scale bars in insets of (a) and (b) 100 nm. Digital FFTs of an entire image are provided as insets in the top right corners of each image.

DOI: 10.1021/acsnano.7b02485
ACS Nano 2017, 11, 7958–7966

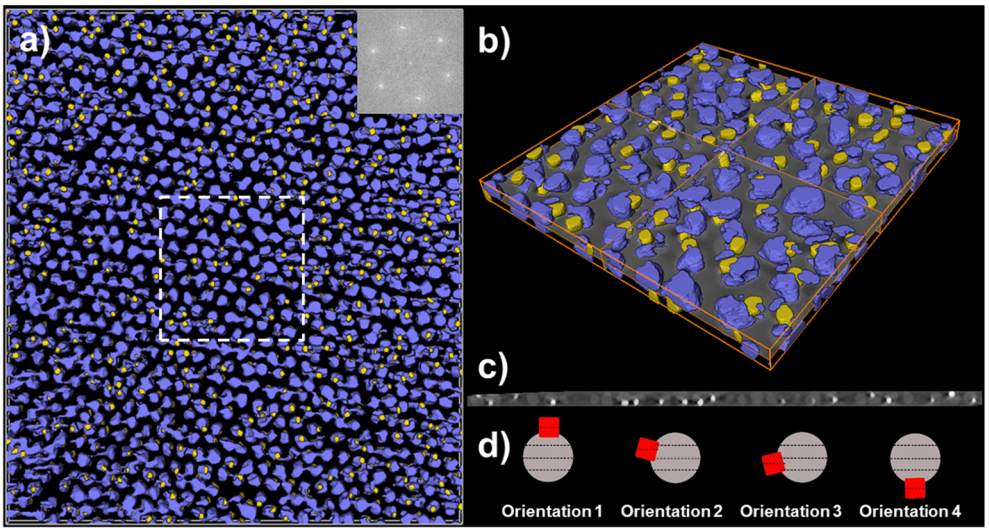

Figure 5. HAADF-STEM tomographic reconstruction of Fe_3O_4–Pt dimer superlattices: (a) an orthographic image of a 3D representation of a subset of the reconstruction with digital FFT as inset and (b) a zoomed in view of Fe_3O_4–Pt dimer superlattices (marked with dashed square in part a), where yellow and indigo blue dots represent Pt and Fe_3O_4, respectively. (c) *XZ* slice view showing that the dimers composing the superlattices are coplanar. (d) Schematic representation of possible orientations of heterodimers.

distributions in the cubic platinum seed and Fe_3O_4 body are well distinguishable as marked with green and red colors in Figure 2b,c. Superimposition of these images yields the reconstructed image (Figure 2f), which is in agreement with Figure 2a. Moreover, we were able to visualize an elemental distribution of sulfur that is a part of the dendritic ligand **6** (Figure 2d). Superimposition of the sulfur and platinum distributions (Figure 2b,d) reveals a major overlap between these two elements that unambiguously proves the selective functionalization of the Pt part with disulfide dendritic ligand **6** (Figure 2e). The schematic representation of the formation of Janus heterodimer with nonpolar dendritic ligand **7** and polar ligand **6** is shown on Figure 3.

Self-Assembly. Self-assembly of particles into layered architectures was achieved on a polar liquid–air interface in a Teflon well. Diethylene glycol was used as the subphase on which a dispersion of the particles in hexanes was deposited. The Teflon well was covered with glass to allow slow evaporation of the hexanes layer. In 2 h, the NPs self-assemble into superlattice films on the liquid–air interface.[63] Thus, obtained solid films were then transferred to a solid substrate by "stamping" (by using a solid wafer/TEM grid to touch from top) and were visualized. Figure 4a shows a schematic representation of all assembly steps including the "stamping" technique.

We first examined the self-assembly of functionalized Fe_3O_4–Pt heterodimers. To our delight, we noticed that the order of the self-assembled layer of particles become progressively better after each ligand exchange step. Self-assembly of the original, as-synthesized Fe_3O_4–Pt heterodimers over liquid–air interface revealed an irregular structure where no long-range order is present (Figure 4b), which is not surprising since the sample has a relatively high polydispersity (14% on Fe_3O_4 and 7.3% on Pt). After ligand exchange with **7**, the interparticle distances (surface to surface) between the NPs increased to 2.4 nm, as the dendron is much larger than the original ligand oleic acid. As seen from TEM image (Figure 4c) of a self-assembled monolayer and bilayer, this step significantly improves the short-range order of such heterodimers.

An improvement of self-assembly properties observed here is believed to be introduced by the large size and monodisperse nature of the dendritic ligand, as it introduces a thick, yet flexible[27] organic shell and is able to counterbalance the size and shape irregularity present in the inorganic parts. Ligand exchange on the platinum part was carried out as the second step using ligands **2**, **4**, and **6**, which were chosen as they would allow tuning polarity of platinum heterodimers. After ligand exchange, samples were examined by the above-mentioned self-assembly technique, and the monolayers were studied. We saw no significant improvement in the assembly properties when ligands **2** and **4** were used (Figures S2 and S3). However, after obtaining Janus particles (functionalizing the Fe_3O_4 part with dendron **7** and the Pt part with dendron **6**), we noticed a further increase in interparticle distance to 4.4 nm and a significant improvement in their self-assembly. Such modification introduced both long-range and short-range order, as can be seen from their self-assembled monolayer (Figure 4d) and bilayer structures (Figure 4i and Figure S4). This finding was further tested using Fe_3O_4–Au heterodimer and dendrons **2**, **4**, and **6**–**9**, where the Fe_3O_4 part was coated with dendron **7** and the Au part was coated with either oleic acid, polar dendrons **2**, **4**, and **6**, or nonpolar dendrons **8** and **9**. Similar to previously observed phenomena, the as-synthesized Fe_3O_4–Au heterodimers show disordered assembly (Figure 4e) that is improved significantly when both the Fe_3O_4 is coated with dendron **7** and the Au parts are coated with either polar dendron **6** (Figure 4g) or nonpolar dendrons **8** and **9** (Figures 4j and 4h). The use of smaller dendrons **2** and **4** did not lead to a significant improvement in self-assembly (Figures S5 and S6).

The enhancement in superlattice film crystallinity can be explained by surface treatment with large dendritic molecules which can influence the assembly process in several ways. First, the whole particle polydispersity of the heterodimer is improved during the two-step ligand exchange process where the surface is coated by large yet monodisperse ligands, that is, the resulting NP dendrimer hybrid is more uniform than the heterodimer was before ligand exchange. Second, the introduction of a thick soft layer may grant the hybrid system

DOI: 10.1021/acsnano.7b02485
ACS Nano 2017, 11, 7958–7966

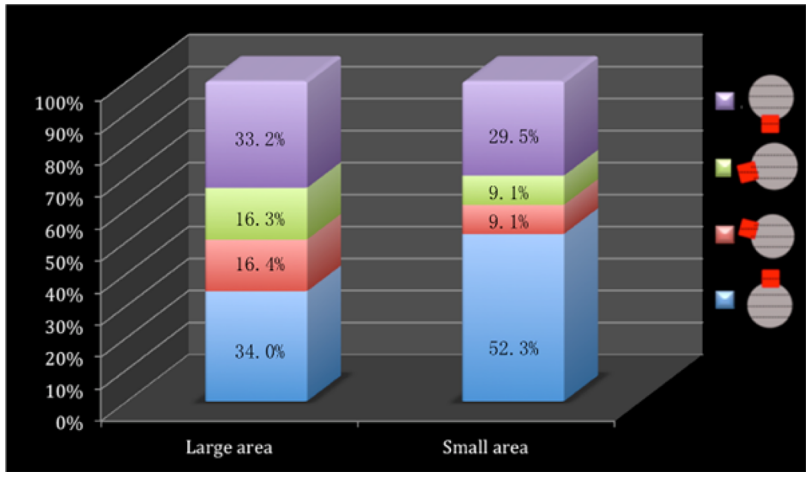

Figure 6. Fe_3O_4–Pt Janus heterodimers orientation quantification.

ability to better accommodate the size irregularity due to the flexible nature of the dendritic ligands or allow rotations during the solvent evaporation process to reduce the in plane size irregularity by pointing the metal part (Pt or Au) out of the assembly plane.

The improvement in whole particle polydispersity can be estimated if the ligand length is accounted during the size polydispersity calculation. For example, in case of the Fe_3O_4–Pt heterodimers, the Fe_3O_4 part (largest component of the heterodimer) has an average diameter of 15.4 ± 2.2 nm, and its polydispersity (based on only inorganic core) is equal to 2.2/15.4 × 100% = 14.2%. As synthesized NPs have ligands with an effective average length of 0.5 nm (obtained by dividing an interparticle separation 1 nm in half), and therefore, the whole particle polydispersity of the as-synthesized same sample is 2.2/(15.4 + 1) = 13.4%.

Dendritic ligands introduce a much larger interparticle separation of 4.4 nm. Therefore, the effective average length of the organic shell is 4.4/2 = 2.2 nm, and the average diameter of the hybrid is 15.4 + 4.4 = 19.8. Considering these numbers, the whole particle polydispersity of the hybrid system (dendronized particles) becomes 2.2/19.8 × 100% = 11%, which is significantly lower (improved) compared to the dispersity of as-synthesized particles calculated based on either whole particles with oleic acid ligands (13.4%) or based on only the inorganic core (14.2%).

To further understand the self-assembly behavior of the dendronized heterodimers, HAADF-STEM tomography was employed. A reconstructed volume of a Fe_3O_4–Pt Janus heterodimer (the Fe_3O_4 part coated with dendron **7** and the Pt part with dendron **6**) superlattice is shown in Figure 5a, together with zoomed in perspective and *XZ* slice view from HAADF-STEM tomographic reconstruction (Figure 5b,c and Supplementary Video), illustrating that the Janus heterodimers composing superlattices are coplanar. The area studied includes 882 particles where the position and the spatial orientation of the particles were explored quantitatively. To study the orientation of individual particles, we considered grouping them into four different orientations where the presence of platinum part is probed in relation to the iron oxide body it is attached to.

Figure 5d demonstrates the four particle orientation classes which were determined by obtaining the spatial orientation of the center point of the platinum cubes with respect to the iron oxide bodies. In a randomly oriented heterodimer superlattice, the orientations 1, 2, 3, and 4 would have equal population. However, the tomographic analysis revealed that, in general, particles prefer the orientations 1 and 4 where the platinum cube is pointing out of particle assembly plane. In comparison, particle orientations 2 and 3 place the platinum part in the assembly plane. Figure 6 presents the percentage of particles found in each orientation within the selected area. The largest area examined (882 particles) shows that more than 2/3 of all particles (67.2%) have either orientation 1 or 4, leaving about 1/3 with orientations 2 and 3 combined. In each case the number of particles that have orientation 1 is almost equal to those found with orientation 4, and the same scenario is seen between orientations 2 and 3 as well. However, the central domain (88 particles) shows an even stronger orientational preference where orientations 1 and 4 together dominate with 82% preference, leaving only 18% that fall into orientations 2 and 3.

The preference of orientation where the platinum part is pointing out of the assembly plane (either up or down) suggests that during the self-assembly process the particles try to increase the packing density. The largest shape irregularity found in the heterodimers is the platinum cube that is attached to the iron oxide body, therefore rotating it out of the plane should reduce the in-plane defects and allow the formation of more ordered crystalline superlattices.

CONCLUSIONS

In conclusion, we find that Janus heterodimers can be obtained by an asymmetric functionalization of Fe_3O_4–Pt and Fe_3O_4–Au heterodimers through sequential ligand exchange steps using dendritic ligands bearing different surface binding groups. This strategy presents an efficient, scalable, and yet simple way to access Janus particles while maintaining dispersibility in organic solvents. Moreover, the surface treatment with dendritic ligands was also found to enhance the self-assembly properties of particles by increasing the whole particle polydispersity and thus counterbalancing the size irregularity of an inorganic core. We foresee the potential utility of heterodimer orthogonal functionalization methodology in biomedical applications such as imaging and/or in catalysis. For example, inorganic subunits can have the potential of bimodal imaging (e.g., magnetic and optical), or one of the components could be functionalized for targeting and/or

DOI: 10.1021/acsnano.7b02485
ACS Nano 2017, 11, 7958–7966

biocompatibility, while the other serves as a reporter. For catalysis, both inorganic parts (and ligands on them) can play a role as is common for the co-optimization of metals catalysts and oxide supports. The orthogonal ligand attachment strategy can be utilized to achieve an orientation control or selective attachment to additional support. In addition, we envision the widespread use of bulky dendritic ligands to overcome the size irregularity present in NPs to achieve improvements in their self-assembly properties and grant access to complex architectures.

METHODS

Materials. 1-Octadecene (technical grade, 90%) was purchased from Acros Organics. Oleic acid (technical grade, 90%) was purchased from Sigma-Aldrich. 2,2-Dimethoxypropane (98+%), bis-MPA (98%), pyridine (reagent), Dowex H^+ ion-exchange resin (200−400 mesh), and oleylamine (80−90%) were purchased from Acros and used without further purification. *N*,*N*′-Dicyclohexylcarbodiimide (DCC, 99%), 4-dimethylaminopyridine (DMAP, 99%), and 11-mercaptoundecan-1-ol **1** (98%) were purchased from Aldrich and used without further purification. Solvents were ACS grade or higher. CH_2Cl_2 was dried over CaH_2 and freshly distilled before used.

Synthesis of Fe_3O_4−Pt and Fe_3O_4−Au Heterodimers. Fe_3O_4−Pt heterodimers were prepared by using platinum nanocubes as seeds following reported recipes.[43] The average size of the platinum nanocube seed was 7.3 ± 0.5 nm (face diagonal length of inorganic part) measured from TEM images (Figure S1). The average size of the Fe_3O_4 body was 15.4 ± 2.2 nm (inorganic part). Fe_3O_4−Au heterodimers were prepared by using gold NPs as seeds following reported recipes.[42] The average size of the gold seeds was 4.9 ± 0.6 nm (inorganic part). The average size of Fe_3O_4 body was 13.0 ± 1.3 nm (inorganic part).

Ligand Exchange on Iron Oxide Part of Heterodimer with Dendron. Ligand exchange on the oleic acid-capped iron oxide part of heterodimers was performed using 1 mL of NPs in hexanes at 10 mg/mL added to 5 mL of chloroform in which was dissolved 10 mg of the replacement ligand phosphonic acid **7**. The reaction mixture was stirred overnight at 35 °C, then the reaction was stopped by precipitation of the NPs with methanol. After centrifugation, the NPs were redispersed in chloroform. This procedure was repeated 3 times to ensure the complete removal of any unbound organic molecules.

Ligand Exchange on Metal (Pt, Au) Part of Heterodimer with Dendrons. Ligand exchange on the oleic acid capped metal (Pt, Au) part of the heterodimers was performed using 1 mL of NPs in hexanes at 10 mg/mL added to 5 mL of chloroform in which was dissolved 10 mg of the corresponding disulfide containing hydrophilic dendron (**2**−**6**). Each reaction was stirred overnight at 35 °C, then the reaction was stopped by precipitation of the NPs with excess methanol. After centrifugation, the NPs were redispersed in chloroform. This procedure was repeated 2 times to ensure the complete removal of any unbound organic molecules.

Techniques. *NMR.* ^{1}H NMR (500 MHz) and ^{13}C NMR (126 MHz) spectra were recorded on a Bruker UNI500 or BIODRX500 NMR spectrometer. ^{1}H and ^{13}C chemical shifts (δ) are reported in ppm, while coupling constants (J) are reported in Hertz (Hz). The multiplicity of signals in ^{1}H NMR spectra is described as "s" (singlet), "d" (doublet), "t" (triplet), "q" (quartet),"p" (pentet), "dd" (doublet of doublets), and "m" (multiplet). All spectra were referenced using solvent residual signals ($CDCl_3$: ^{1}H, δ 7.27 ppm; ^{13}C, δ 77.2 ppm).[64] Reaction progress was monitored by thin-layer chromatography using silica gel-coated plates or ^{1}H NMR. Compounds were purified by filtration, precipitation, crystallization, or flash column chromatography using silica gel (Acros Organics, 90 Å, 35−70 μm) as indicated in corresponding procedures.

Mass Spectroscopy. Matrix-assisted laser desorption/ionization time-of-flight (MALDI-TOF) mass spectrometry was performed on a Bruker Ultraflex III (Maldi-Tof-Tof) mass spectrometer using dithranol as matrix.

Electron Microscopy. Transmission electron microscopy (TEM) micrographs were collected using a JEOL 1400 microscope operated at 120 kV. The TEM was calibrated using a MAG*I*CAL TEM calibration standard.

2D and 3D High-Angle Annular Dark-Field Scanning Transmission Electron Microscopy (HAADF-STEM) Measurements. Both 2D and 3D HAADF-STEM measurements were performed using a FEI Talos F200X transmission electron microscope, equipped with a high-brightness field emission gun (X-FEG) and operated at 200 kV. A Fischione model 2020 single tilt holder was used for the acquisition of the tilt series within a tilt range from −66° to +68°, and an increment of 2° was used. Unwanted diffraction contrast was avoided by applying HAADF-STEM imaging. The tilt series was aligned using cross-correlation routines implemented in Fiji (http://fiji.sc/) and TomoJ.[65] The reconstruction was performed using the simultaneous iterative reconstruction technique (SIRT)[66] algorithm in TomoJ 2.31. Segmentation of the tomograms was carried out mainly through thresholding and marker-based watershed transformation in Avizo 9 (FEI Visualization Sciences Group, http://www.fei.com/software/avizo-3d-for-materials-science/) as well as 3D volume rendering of reconstructed superlattices.

2D Energy Dispersive X-ray Spectroscopy (EDX) Chemical Mapping Measurements. 2D EDX chemical mapping measurements were performed using a FEI Talos F200X transmission electron microscope, equipped with a high-brightness field emission gun (X-FEG) and a Super-X G2 EDX detector operated at 200 kV. Images and elemental EDX maps were acquired using Bruker Esprit analytical and imaging software in scanning transmission mode. Elemental EDX maps of 802 × 801 pixels were acquired with a 15 min acquisition time to get a good signal-to-noise ratio.

ASSOCIATED CONTENT

Supporting Information

Following files are available free of charge. The Supporting Information is available free of charge on the ACS Publications website at DOI: 10.1021/acsnano.7b02485.

Full characterization of organic compounds, additional microscopy, supporting spectroscopy, and supplemental video (PDF)

XZ slice view from HAADF-STEM tomographic reconstruction (AVI)

AUTHOR INFORMATION

Corresponding Author

*E-mail: cbmurray@sas.upenn.edu.

ORCID

Davit Jishkariani: 0000-0003-3771-2645

Yaoting Wu: 0000-0002-4363-9870

Author Contributions

⊥These authors contributed equally

Notes

The authors declare the following competing financial interest(s): Aspects of this work have been included in a U.S. provisional patent filing.

ACKNOWLEDGMENTS

This work was supported by the CNRS-UPENN-SOLVAY through the Complex Assemblies of Soft Matter Laboratory (COMPASS), in partnership with the University of Pennsylvania's NSF MRSEC under award no. DMR-112090. C.B.M. acknowledges the Richard Perry University Professorship at the University of Pennsylvania. D.W. and A.v.B. acknowledge partial funding from the European Research Council under the European Union's Seventh Framework Programme (FP-2007-

DOI: 10.1021/acsnano.7b02485
ACS Nano 2017, 11, 7958−7966

2013)/ERC Advanced Grant Agreement 291667 HierarSACol. The authors thank EM square in Utrecht University for the access to the microscopes. D.J. acknowledges Martín Citoler-Saumell for helpful discussions.

REFERENCES

(1) *Nanoparticles: Building Blocks for Nanotechnology*; Rotello, V. M., Ed.; Springer Science & Business Media: New York, 2004.
(2) Daniel, M.-C.; Astruc, D. Gold Nanoparticles: Assembly, Supramolecular Chemistry, Quantum-Size-Related Properties, and Applications toward Biology, Catalysis, and Nanotechnology. *Chem. Rev.* **2004**, *104*, 293−346.
(3) Eustis, S.; el-Sayed, M. A. Why Gold Nanoparticles Are More Precious than Pretty Gold: Noble Metal Surface Plasmon Resonance and Its Enhancement of the Radiative and Nonradiative Properties of Nanocrystals of Different Shapes. *Chem. Soc. Rev.* **2006**, *35*, 209−217.
(4) Choi, J.-H.; Wang, H.; Oh, S. J.; Paik, T.; Sung, P.; Sung, J.; Ye, X.; Zhao, T.; Diroll, B. T.; Murray, C. B.; Kagan, C. R. Exploiting the Colloidal Nanocrystal Library to Construct Electronic Devices. *Science* **2016**, *352*, 205−208.
(5) Kovalenko, M. V.; Manna, L.; Cabot, A.; Hens, Z.; Talapin, D. V.; Kagan, C. R.; Klimov, V. I.; Rogach, A. L.; Reiss, P.; Milliron, D. J.; Guyot-Sionnnest, P.; Konstantatos, G.; Parak, W. J.; Hyeon, T.; Korgel, B. A.; Murray, C. B.; Heiss, W. Prospects of Nanoscience with Nanocrystals. *ACS Nano* **2015**, *9*, 1012−1057.
(6) Sharma, P.; Brown, S.; Walter, G.; Santra, S.; Moudgil, B. Nanoparticles for Bioimaging. *Adv. Colloid Interface Sci.* **2006**, *123*−*126*, 471−485.
(7) Erathodiyil, N.; Ying, J. Y. Functionalization of Inorganic Nanoparticles for Bioimaging Applications. *Acc. Chem. Res.* **2011**, *44*, 925−935.
(8) Chappert, C.; Fert, A.; Van Dau, F. N. The Emergence of Spin Electronics in Data Storage. *Nat. Mater.* **2007**, *6*, 813−823.
(9) Terris, B. D.; Thomson, T. Nanofabricated and Self-Assembled Magnetic Structures as Data Storage Media. *J. Phys. D: Appl. Phys.* **2005**, *38*, R199−R222.
(10) Saha, K.; Agasti, S. S.; Kim, C.; Li, X.; Rotello, V. M. Gold Nanoparticles in Chemical and Biological Sensing. *Chem. Rev.* **2012**, *112*, 2739−2779.
(11) Astruc, D.; Lu, F.; Aranzaes, J. R. Nanoparticles as Recyclable Catalysts: The Frontier between Homogeneous and Heterogeneous Catalysis. *Angew. Chem., Int. Ed.* **2005**, *44*, 7852−7872.
(12) Yan, N.; Xiao, C.; Kou, Y. Transition Metal Nanoparticle Catalysis in Green Solvents. *Coord. Chem. Rev.* **2010**, *254*, 1179−1218.
(13) Diroll, B. T.; Jishkariani, D.; Cargnello, M.; Murray, C. B.; Donnio, B. Polycatenar Ligand Control of the Synthesis and Self-Assembly of Colloidal Nanocrystals. *J. Am. Chem. Soc.* **2016**, *138*, 10508−10515.
(14) Thanh, N. T. K.; Maclean, N.; Mahiddine, S. Mechanisms of Nucleation and Growth of Nanoparticles in Solution. *Chem. Rev.* **2014**, *114*, 7610−7630.
(15) Cortie, M. B.; McDonagh, A. M. Synthesis and Optical Properties of Hybrid and Alloy Plasmonic Nanoparticles. *Chem. Rev.* **2011**, *111*, 3713−3735.
(16) Dahl, J. A.; Maddux, B. L. S.; Hutchison, J. E. Toward Greener Nanosynthesis. *Chem. Rev.* **2007**, *107*, 2228−2269.
(17) Jishkariani, D.; Diroll, B. T.; Cargnello, M.; Klein, D. R.; Hough, L. A.; Murray, C. B.; Donnio, B. Dendron-Mediated Engineering of Interparticle Separation and Self-Assembly in Dendronized Gold Nanoparticles Superlattices. *J. Am. Chem. Soc.* **2015**, *137*, 10728−10734.
(18) Fleutot, S.; Nealon, G. L.; Pauly, M.; Pichon, B. P.; Leuvrey, C.; Drillon, M.; Gallani, J.-L.; Guillon, D.; Donnio, B.; Begin-Colin, S. Spacing-Dependent Dipolar Interactions in Dendronized Magnetic Iron Oxide Nanoparticle 2D Arrays and Powders. *Nanoscale* **2013**, *5*, 1507−1516.
(19) Fafarman, A. T.; Koh, W.; Diroll, B. T.; Kim, D. K.; Ko, D.-K.; Oh, S. J.; Ye, X.; Doan-Nguyen, V.; Crump, M. R.; Reifsnyder, D. C.; Murray, C. B.; Kagan, C. R. Thiocyanate-Capped Nanocrystal Colloids: Vibrational Reporter of Surface Chemistry and Solution-Based Route to Enhanced Coupling in Nanocrystal Solids. *J. Am. Chem. Soc.* **2011**, *133*, 15753−15761.
(20) Malassis, L.; Jishkariani, D.; Murray, C. B.; Donnio, B. Dendronization-Induced Phase-Transfer, Stabilization and Self-Assembly of Large Colloidal Au Nanoparticles. *Nanoscale* **2016**, *8*, 13192−13198.
(21) Alkilany, A. M.; Yaseen, A. I. B.; Park, J.; Eller, J. R.; Murphy, C. J. Facile Phase Transfer of Gold Nanoparticles from Aqueous Solution to Organic Solvents with Thiolated Poly(ethylene Glycol). *RSC Adv.* **2014**, *4*, 52676−52679.
(22) Macfarlane, R. J.; Lee, B.; Jones, M. R.; Harris, N.; Schatz, G. C.; Mirkin, C. A. Nanoparticle Superlattice Engineering with DNA. *Science* **2011**, *334*, 204−208.
(23) Zhang, C.; Macfarlane, R. J.; Young, K. L.; Choi, C. H. J.; Hao, L.; Auyeung, E.; Liu, G.; Zhou, X.; Mirkin, C. A. A General Approach to DNA-Programmable Atom Equivalents. *Nat. Mater.* **2013**, *12*, 741−746.
(24) Brust, M.; Walker, M.; Bethell, D.; Schiffrin, D. J.; Whyman, R. Synthesis of Thiol-Derivatised Gold Nanoparticles in a Two-Phase Liquid-Liquid System. *J. Chem. Soc., Chem. Commun.* **1994**, *0*, 801−802.
(25) Mirkin, C. A.; Letsinger, R. L.; Mucic, R. C.; Storhoff, J. J. A DNA-Based Method for Rationally Assembling Nanoparticles into Macroscopic Materials. *Nature* **1996**, *382*, 607−609.
(26) Hanemann, T.; Szabó, D. V. Polymer-Nanoparticle Composites: From Synthesis to Modern Applications. *Materials* **2010**, *3*, 3468−3517.
(27) Diroll, B. T.; Weigandt, K. M.; Jishkariani, D.; Cargnello, M.; Murphy, R. J.; Hough, L. A.; Murray, C. B.; Donnio, B. Quantifying "Softness" of Organic Coatings on Gold Nanoparticles Using Correlated Small-Angle X-Ray and Neutron Scattering. *Nano Lett.* **2015**, *15*, 8008−8012.
(28) Esipova, T. V.; Ye, X.; Collins, J. E.; Sakadžić, S.; Mandeville, E. T.; Murray, C. B.; Vinogradov, S. A. Dendritic Upconverting Nanoparticles Enable *in Vivo* Multiphoton Microscopy with Low-Power Continuous Wave Sources. *Proc. Natl. Acad. Sci. U. S. A.* **2012**, *109*, 20826−20831.
(29) Lattuada, M.; Hatton, T. A. Synthesis, Properties and Applications of Janus Nanoparticles. *Nano Today* **2011**, *6*, 286−308.
(30) Walther, A.; Müller, A. H. E. Janus Particles: Synthesis, Self-Assembly, Physical Properties, and Applications. *Chem. Rev.* **2013**, *113*, 5194−5261.
(31) Chen, Q.; Whitmer, J. K.; Jiang, S.; Bae, S. C.; Luijten, E.; Granick, S. Supracolloidal Reaction Kinetics of Janus Spheres. *Science* **2011**, *331*, 199−202.
(32) Xuan, M.; Wu, Z.; Shao, J.; Dai, L.; Si, T.; He, Q. Near Infrared Light-Powered Janus Mesoporous Silica Nanoparticle Motors. *J. Am. Chem. Soc.* **2016**, *138*, 6492−6497.
(33) Jang, S. G.; Kim, S.-H.; Lee, S. Y.; Jeong, W. C.; Yang, S.-M. Facile Synthesis of Core-Shell and Janus Particles via 2-D Dendritic Growth of Gold Film. *J. Colloid Interface Sci.* **2010**, *350*, 387−395.
(34) Koo, H. Y.; Yi, D. K.; Yoo, S. J.; Kim, D.-Y. A Snowman-like Array of Colloidal Dimers for Antireflecting Surfaces. *Adv. Mater.* **2004**, *16*, 274−277.
(35) Cha, B. G.; Piao, Y.; Kim, J. Asymmetric Nanoparticle Assembly via Simple Mechanical Pressing Using Relative Hardness of Materials. *Mater. Res. Bull.* **2015**, *70*, 424−429.
(36) Bradley, L. C.; Stebe, K. J.; Lee, D. Clickable Janus Particles. *J. Am. Chem. Soc.* **2016**, *138*, 11437−11440.
(37) Pawar, A. B.; Kretzschmar, I. Fabrication, Assembly, and Application of Patchy Particles. *Macromol. Rapid Commun.* **2010**, *31*, 150−168.
(38) Song, Y.; Chen, S. Janus Nanoparticles: Preparation, Characterization, and Applications. *Chem. - Asian J.* **2014**, *9*, 418−430.
(39) Hu, J.; Zhou, S.; Sun, Y.; Fang, X.; Wu, L. Fabrication, Properties and Applications of Janus Particles. *Chem. Soc. Rev.* **2012**, *41*, 4356−4378.

DOI: 10.1021/acsnano.7b02485
ACS Nano 2017, 11, 7958−7966

(40) Zeng, H.; Sun, S. Syntheses, Properties, and Potential Applications of Multicomponent Magnetic Nanoparticles. *Adv. Funct. Mater.* **2008**, *18*, 391−400.
(41) Brown, L. V.; Sobhani, H.; Lassiter, J. B.; Nordlander, P.; Halas, N. J. Heterodimers: Plasmonic Properties of Mismatched Nanoparticle Pairs. *ACS Nano* **2010**, *4*, 819−832.
(42) Jiang, G.; Huang, Y.; Zhang, S.; Zhu, H.; Wu, Z.; Sun, S. Controlled Synthesis of Au−Fe Heterodimer Nanoparticles and Their Conversion into Au−Fe_3O_4 Heterostructured Nanoparticles. *Nanoscale* **2016**, *8*, 17947−17952.
(43) Hodges, J. M.; Morse, J. R.; Williams, M. E.; Schaak, R. E. Microscopic Investigation of Chemoselectivity in Ag-Pt-Fe_3O_4 Heterotrimer Formation: Mechanistic Insights and Implications for Controlling High-Order Hybrid Nanoparticle Morphology. *J. Am. Chem. Soc.* **2015**, *137*, 15493−15500.
(44) Gu, H.; Zheng, R.; Zhang, X.; Xu, B. Facile One-Pot Synthesis of Bifunctional Heterodimers of Nanoparticles: A Conjugate of Quantum Dot and Magnetic Nanoparticles. *J. Am. Chem. Soc.* **2004**, *126*, 5664−5665.
(45) Wang, C.; Xu, C.; Zeng, H.; Sun, S. Recent Progress in Syntheses and Applications of Dumbbell-like Nanoparticles. *Adv. Mater.* **2009**, *21*, 3045−3052.
(46) Shi, W.; Zeng, H.; Sahoo, Y.; Ohulchanskyy, T. Y.; Ding, Y.; Wang, Z. L.; Swihart, M.; Prasad, P. N. General Approach to Binary and Ternary Hybrid Nanocrystals. *Nano Lett.* **2006**, *6*, 875−881.
(47) Xu, C.; Wang, B.; Sun, S. Dumbbell-like Au−Fe3O4 Nanoparticles for Target-Specific Platin Delivery. *J. Am. Chem. Soc.* **2009**, *131*, 4216−4217.
(48) Yang, M.; Cheng, K.; Qi, S.; Liu, H.; Jiang, Y.; Jiang, H.; Li, J.; Chen, K.; Zhang, H.; Cheng, Z. Affibody Modified and Radiolabeled gold−Iron Oxide Hetero-Nanostructures for Tumor PET, Optical and MR Imaging. *Biomaterials* **2013**, *34*, 2796−2806.
(49) Gu, H.; Yang, Z.; Gao, J.; Chang, C. K.; Xu, B. Heterodimers of Nanoparticles: Formation at a Liquid-Liquid Interface and Particle-Specific Surface Modification by Functional Molecules. *J. Am. Chem. Soc.* **2005**, *127*, 34−35.
(50) Gao, J.; Gu, H.; Xu, B. Multifunctional Magnetic Nanoparticles: Design, Synthesis, and Biomedical Applications. *Acc. Chem. Res.* **2009**, *42*, 1097−1107.
(51) Davis, K.; Qi, B.; Witmer, M.; Kitchens, C. L.; Powell, B. A.; Mefford, O. T. Quantitative Measurement of Ligand Exchange on Iron Oxides via Radiolabeled Oleic Acid. *Langmuir* **2014**, *30*, 10918−10925.
(52) Fleutot, S.; Nealon, G. L.; Pauly, M.; Pichon, B. P.; Leuvrey, C.; Drillon, M.; Gallani, J.-L.; Guillon, D.; Donnio, B.; Begin-Colin, S. Spacing-Dependent Dipolar Interactions in Dendronized Magnetic Iron Oxide Nanoparticle 2D Arrays and Powders. *Nanoscale* **2013**, *5*, 1507−1516.
(53) Petrovykh, D. Y.; Kimura-Suda, H.; Opdahl, A.; Richter, L. J.; Tarlov, M. J.; Whitman, L. J. Alkanethiols on Platinum: Multicomponent Self-Assembled Monolayers. *Langmuir* **2006**, *22*, 2578−2587.
(54) Love, J. C.; Estroff, L. A.; Kriebel, J. K.; Nuzzo, R. G.; Whitesides, G. M. Self-Assembled Monolayers of Thiolates on Metals as a Form of Nanotechnology. *Chem. Rev.* **2005**, *105*, 1103−1169.
(55) Bosman, A. W.; Janssen, H. M.; Meijer, E. W. About Dendrimers: Structure, Physical Properties, and Applications. *Chem. Rev.* **1999**, *99*, 1665−1688.
(56) Newkome, G. R.; Moorefield, C. N.; Vögtle, F. *Dendrimers and Dendrons*; Wiley-VCH Verlag GmbH & Co. KGaA: Weinheim, 2001.
(57) Hawker, C. J.; Malmström, E. E.; Frank, C. W.; Kampf, J. P. Exact Linear Analogs of Dendritic Polyether Macromolecules: Design, Synthesis, and Unique Properties. *J. Am. Chem. Soc.* **1997**, *119*, 9903−9904.
(58) Luo, L.; Zhang, L.; Duan, Z.; Lapp, A. S.; Henkelman, G.; Crooks, R. M. Efficient CO Oxidation Using Dendrimer-Encapsulated Pt Nanoparticles Activated with < 2% Cu Surface Atoms. *ACS Nano* **2016**, *10*, 8760−8769.
(59) Jishkariani, D.; MacDermaid, C. M.; Timsina, Y. N.; Grama, S.; Gillani, S. S.; Divar, M.; Yadavalli, S. S.; Moussodia, R.-O.; Leowanawat, P.; Camacho, A. M. B.; Walter, R.; Goulian, M.; Klein, M. L.; Percec, V. Self-Interrupted Synthesis of Sterically Hindered Aliphatic Polyamide Dendrimers. *Proc. Natl. Acad. Sci. U. S. A.* **2017**, *114*, E2275−E2284.
(60) Ihre, H.; Padilla De Jesús, O. L.; Fréchet, J. M. J. Fast and Convenient Divergent Synthesis of Aliphatic Ester Dendrimers by Anhydride Coupling. *J. Am. Chem. Soc.* **2001**, *123*, 5908−5917.
(61) Ihre, H.; Hult, A.; Söderlind, E. Synthesis, Characterization, and 1H NMR Self-Diffusion Studies of Dendritic Aliphatic Polyesters Based on 2,2-Bis(hydroxymethyl)propionic Acid and 1,1,1-Tris-(hydroxyphenyl)ethane. *J. Am. Chem. Soc.* **1996**, *118*, 6388−6395.
(62) Jishkariani, D.; Lee, J. D.; Yun, H.; Paik, T.; Kikkawa, J. M.; Kagan, C. R.; Donnio, B.; Murray, C. B. Dendritic Effect and Magnetic Permeability in Dendron Coated Nickel and Manganese Zinc Ferrite Nanoparticles. *Nanoscale*, submitted **2017**.
(63) Dong, A.; Chen, J.; Vora, P. M.; Kikkawa, J. M.; Murray, C. B. Binary Nanocrystal Superlattice Membranes Self-Assembled at the Liquid-Air Interface. *Nature* **2010**, *466*, 474−477.
(64) Gottlieb, H. E.; Kotlyar, V.; Nudelman, A. NMR Chemical Shifts of Common Laboratory Solvents as Trace Impurities. *J. Org. Chem.* **1997**, *62*, 7512−7515.
(65) MessaoudiI, C.; Boudier, T.; Sorzano, C. O. S.; Marco, S. TomoJ: Tomography Software for Three-Dimensional Reconstruction in Transmission Electron Microscopy. *BMC Bioinf.* **2007**, *8*, 288−296.
(66) Gilbert, P. Iterative Methods for the Three-Dimensional Reconstruction of an Object from Projections. *J. Theor. Biol.* **1972**, *36*, 105−117.

DOI: 10.1021/acsnano.7b02485
ACS Nano 2017, 11, 7958−7966